Research Square

Preprints are preliminary reports that have not undergone peer review.
They should not be considered conclusive, used to inform clinical practice,
or referenced by the media as validated information.

The impact of land use and land cover on land surface temperature in an Indian riverine town over a decade and how it varied post-lockdown

Shubhayan Roy Chowdhury
Jadavpur University
Prerana Bhaumik
Jadavpur University
Satiprasad Sahoo
International Institute of Geospatial and Technology
Abhra Chanda
Jadavpur University
Trinh Trong Nguyen
ntdthuyduytan@gmail.com
HUTECH Institute of Applied Sciences
Ismail Elkhrachy
Najran University
Nguyen Nguyet Minh
Van Lang University

Research Article

Keywords: Land use land cover, land surface temperature, Covid_19, Spectral indices, Multiple regression analysis, Balurghat

Posted Date: July 11th, 2023

DOI: https://doi.org/10.21203/rs.3.rs-3089557/v1

License: This work is licensed under a Creative Commons Attribution 4.0 International License. Read Full License

Abstract

In towns and cities in developing countries, negligence in consistently regulating the growth of urban sprawl is commonplace. The purpose of the study was to analyze spatiotemporal changes in land use land cover (LULC) and their impact on land surface temperature (LST) in Balurghat, Dakshin Dinajpur district, West Bengal, India. The results revealed a decrease in the vegetation cover (64–44%) and an increase in the built-up area (14–39%) from 2012 to 2022. Over the study period, built-up regions and bare land had the highest temperatures, ranging from 20.6°C to 24.96°C, and waterbodies had the lowest temperatures, ranging from 17.85°C to 20.47°C. From 2012 to 2017, LST exhibited an increasing trend. However, after the lockdown, LST declined slightly in 2022. The mean LST variations in the study area from 2012 to 2022, presenting a pre- and post-pandemic scenario, were also highlighted in this study. Furthermore, this study emphasized the correlation analysis between LST and four spectral indices, which are the Normalized Difference Built-up Index (NDBI), the Normalized Difference Vegetation Index (NDVI), the Soil Adjusted Vegetation Index (SAVI), and the Modified Normalized Difference Water Index (MNDWI). Multiple linear regression (MLR) containing NDVI and MNDWI with LST has been consistently the best-fit model for 2012, 2017 and 2022. These models have been established using various statistical tools, primarily the Akaike information criterion (AIC) model selection and the Inflation Factor (VIF). The results provide a framework for sustainable urban design and development, which can serve as a resource for policymakers and increase public understanding.

1 Introduction

Most non-agricultural enterprises, such as building urban facilities, expanding the transportation network, and providing many other conveniences, are concentrated in urban areas. A geographical region is affected by economic and social interactions that come from urban growth and have an effect on the LULC of the study area (Neog et al., 2019). Urbanization is a form of development that has raised national and international issues, and humanity cannot disregard the effects of its implementation since they have taken hold in a hostile environment (Eena et al., 2020). The result of the urbanization process is the transformation of the environmental landscape into anthropogenic surfaces, or land that has been covered with paved structures like buildings, highways, and parking lots (Ishola et al., 2016). Once urban development replaces vegetation, various climate variables are also significantly altered (Kometa & Akoh, 2012). Rapid urbanization may have significant adverse effects on numerous natural factors, notably on land and water, even though it has crucial consequences for changes in demographic characteristics and the physical landscape. Therefore, to adapt to environmental changes and promote sustainable development, a full understanding of the shift in LULC is required. This is especially true given that the vast majority of metropolitan areas throughout the world have seen substantial changes in their land cover over time (Battista & Vollaro, 2017). Few landscapes still exist in their original state, according to the current land-use system. This land-use system is imperative in creating a connection between the biosphere and the socioeconomic structure. Variations in LULC are thought to be one of the major forces driving global change that affects the Earth and its environment (AL-Shammari et al., 2021; Uddin et al., 2022). Land use has changed dramatically as a consequence of anthropogenic forces, and as time goes on, humans' impact on the environment is becoming more obvious, leading to a shift in the land use pattern that can be seen throughout time. Anthropogenic activities have a significant impact on urban environments, according to research (Lundholm & Richardson, 2010). Surface-temperature increases as a result of LULC change brought on by human influence (Rahaman et al., 2020). As a result, to segregate human activity and biogeographical diversity, spatially explicit LULC is required (Turner et al., 2007). GIS and remote sensing are efficient methods for generating precise and timely data on the spatial distribution of changes in LULC over large areas (Carlson & Sanchez-Azofeifa, 1999; Dezso et al., 2005). In this study, LULC changes in the study area were analyzed by using satellite imagery and GIS and subjected to the change detection comparison approach.

The properties of many land-surface types have recently changed as a result of growing urbanization (Li et al., 2017). This also caused a shift in the temperature of the land. LST is dependent on changing surface conditions and is an excellent indication of energy segmentation in the area where land and air meet, so the LST is regarded as a crucial metric (Hao et al., 2016). The LST is also employed in a wide range of disciplines, including evapotranspiration, vegetation, the hydrological cycle, and climate change (Kalma et al., 2008). It is the primary variable that is influenced by the characteristics of the land surface, including land use, land cover, vegetation, and the permeability of the soil surface (Mathew et al., 2018). Numerous investigations have been conducted to investigate how variables in LULC affect the LST (Nega & Balew, 2022; Thakur et al., 2021; Vani & Prasad, 2020). The LST can be quantified using two different sorts of techniques, including the traditional way and the remote sensing methodology. The LST is computed by meteorological stations in the traditional method, whereas remote sensing provides for its estimation using a model of surface energy balance (Daou et al., 2012). LST is a decisive factor in the microclimate and radiation transport inside the atmosphere. To evaluate the spatiotemporal fluctuations in the LST, GIS and RS techniques combined with ground-truthing field data are advocated (Rajendran & Mani, 2015). Since the development of thermal remote sensing, LST data has been made accessible from several satellite sensors that monitor different areas of the earth's surface, including Landsat, moderate resolution imaging spectroradiometer (MODIS), and advanced spaceborne thermal emission and reflection radiometer (ASTER). Thermal photography offers comprehensive geographical coverage at different temporal scales, in contrast to air temperatures measured by meteorological stations (Myint et al., 2013). Furthermore, LST obtained from remote sensing images may be more accurate in displaying the warmest and coolest regions than temperature data gathered from an urban weather station (Nichol & Hang, 2012). The parameters of LULC are also directly influenced by the LST (Quattrochi & Luvall, 1999). The growing trend in the urban environment's temperature is mostly caused by anthropogenic emissions, aerosols, and pollutants; therefore, the lockdown's lower concentrations would cause a greater disparity in thermal radiation between urban and rural regions (Shikwambana et al., 2021). The COVID-19 lockdown provides a chance to investigate the effects of decreased air pollution and reduced heat output from surface vehicles on LST. Hence, the capacity to characterize the fluctuation of LST is facilitated by the use of earth observation satellite data. The purpose of this study was to assess variations in LST over the city of Balurghat during the pre-and post-lockdown periods using satellite-derived LST data. on a reliable study of the relationship between the change of LULC and LST.

Various researchers regard the vegetation index as one of the most important factors for mapping agricultural fields, forecasting weather patterns, quantifying biomass and crop productivity, assessing drought conditions, and assessing vegetation vibrancy (Chakraborty & Sehgal, 2010; Narasimhan & Srinivasan, 2005). The most straightforward, effective, and widely used one is the NDVI (Liu & Huete, 1995). The correlations between the LST and NDVI in the Chinese city of Shanghai have been established using satellite data, and GIS and RS tools have reported that these connections are useful in identifying

the climatic impacts on the environment (Yue et al., 2007). To establish a connection between LST and NDVI, the majority of researchers are now using thermal infrared remote sensing (Li et al., 2017; Stroppiana et al., 2014). Successful recent analysis has also been carried out on the spatial-temporal association of LST-NDVI in tropical India, e.g., Ahmedabad(Mathew et al., 2018), Jaipur (Khandelwal et al., 2017), Kalaburagi (Kumar & Shekhar, 2015), Noida (Kikon et al., 2016), and Lucknow (P. Singh et al., 2017). NDBI is a crucial spectral index that strongly corresponds to LST(Guha et al., 2018). Several recent studies (Alexander, 2020; Balew & Korme, 2020; Son et al., 2020) assess the LST-NDBI correlation on various types of LULC in a tropical environment. MNDWI, like other land surfaces, is used to improve water bodies and has an antagonistic relationship with LST (H. Xu, 2006).

In this study, the four remote sensing indices: NDVI, SAVI, MNDWI, and NDBI were selected and the correlation coefficients (R) between the LST and these spectral indices were conducted to determine strongly associated indices with LST. This approach is used to reduce the total number of variables and to facilitate a simpler simulation procedure. To comprehend how LULC affects the LST in the pre-monsoon season in the city of Balurghat, it is essential to analyze the link between LULC and LST. For the city of Balurghat, the effects of LULC changes on LST, however, have not been thoroughly researched and documented. There were a few investigations done in the city of Balurghat (Kundu, 2018; B. Singh & Sarkar, 2020). Therefore, this study was carried out to close these information gaps and focused on offering some details. The results of this study can also be used by other researchers as a starting point for conducting future studies on pertinent topics. Additionally, it offers novel information to help researchers and experts better comprehend the dynamics of LULC, as well as their effects on LST. Also, it enables us to inform the neighborhood about the significance of preventing future environmental degradation. The major goal of this study was to identify changes in LULC and their effects on LST during 10 years (2012–2022) in the city of Balurghat, district of Dakshin Dinajpur, West Bengal, India.

The following particular goals were developed to fulfil this overarching goal:

1. Examine the spatiotemporal range and dynamics of LULC in Balurghat town.
2. Examine the LST under various LULC categories.
3. Analyze the fluctuations of LST in the pre- and post-lockdown periods.
4. Analyze the link between various spectral indices and LST for 2012, 2017, and 2022.

2 Materials and methods

2.1 Study area

The town of Balurghat is located between 25°13’0" N and 88°47’0" E within the Dakshin Dinajpur district of West Bengal, India (Fig. 1). The silty-loamy to sandy-loamy soil and suitable weather may be the reasons it is agriculturally sound. Additionally, the river Atrai flows through Balurghat, creating a broad riverbed with good soil before reaching the river Brahmaputra in Bangladesh (Kamilya et al., 2015). The border between India and Bangladesh is only three kilometers away from this major metropolis. The city is connected by roads and trains and is located 434 kilometers from Kolkata, the state headquarters (B. Singh & Sarkar, 2020). It covers an area of 10.6 km^2 and comprises 25 wards, having a total population of 164,816 (Census of India, 2022). The town has a humid subtropical climate with average annual temperatures ranging from 34°C in the summer to 16°C in the winter, with an average annual rainfall of 323 mm. The political reasons for the country's split in 1947 and again in 1971 as a result of the Bangladesh Liberation War are the significant aspects that contributed to the formation of the Balurghat town that exists today. At present, the city is governed by the Balurghat Municipal Corporation Board.

2.2 Data used

In this study, data from the Landsat Multispectral Scanner (MSS) and the Enhanced Thematic Mapper Plus (ETM+), were collected in 2012, 2017, and 2022 respectively. On the United States Geological Survey's (USGS) website, the satellite images are publicly available. The characteristics of the satellite data utilized in the investigation are presented in Table 1.

Table 1
The characteristics of satellite data used in the city of Balurghat

Landsat image	Sensor_ID	Date of acquisition	Path _Row	No. of bands	Resolution (m)	Source
Landsat 7	ETM+	2012-02-04	169 & 53	8	30	USGS
Landsat 8	OLI_TIRS	2017-02-25	169 & 53	11	30	USGS
Landsat 8	OLI_TIRS	2022-02-15	169 & 53	11	30	USGS

A flow chart is provided to comprehend the study's approach (Fig. 2).

2.3 LULC mapping

The LU/LC changes that occurred over the study periods (2012, 2017, 2022) were detected and classified by using Landsat 7 and Landsat 8 images (Dissanayake et al., 2019). Waterbody, vegetation, built-up area, sand, bare land, and agricultural fallow land are among the six LU/LC classes that were used to describe Balurghat City. The LULC maps were created using the maximum likelihood classification algorithm, and this algorithm is used to extract data from every multispectral band and categories the image's cells into user-defined categories. One of the most crucial steps in the image classification process is validation, which assesses how well an algorithm has classified the various objects in an image. For validating the classification, the accuracy assessment has been done (Bogoliubova & Tymków, 2014).

2.4 Retrieval technique for LST

In this study, the LST of the city of Balurghat was estimated using the thermal infrared bands of several Landsat images (band 6 of Landsat 7 ETM+, and band 10 of Landsat 8). The data of Landsat 7 and Landsat 8 are available on the Earth Explorer website free of charge. Leveraging Band 6 for Landsat 7 ETM + and Band 10 for Landsat 8 OLI/TIRS satellites, the LST values were computed using Landsat thermal images (Song et al., 2014). The subsequent processes are involved in LST retrieval. Using the following calculation, the DN values were converted back to radiance units by using Eq. (3) (Alipour et al., 2003; Donnell et al., 2003)

$$\text{Radiance}\,(\mathrm{L}_\lambda) = \mathrm{ga\dot{i}n}{*}\mathrm{DN} + \text{offset}$$ (Eq. 3)

Which may also be expressed as Eq. (4)

$$\mathrm{L}_\lambda = \frac{(\mathrm{L_{MAX}} - \mathrm{L_{MIN}})}{(\mathrm{Q_{CALMAX}} - \mathrm{Q_{CALMIN}})} * (\mathrm{Q_{CAL}} - \mathrm{Q_{CALMIN}}) + \mathrm{L_{MIN}}$$ (Eq. 4)

Where L_{MAX} and L_{MIN} are spectral values included in the Landsat pictures' metadata. The calibration values of pixels for Q_{CALMAX} and Q_{CALMIN} have been found from Landsat image metadata.

For Landsat 8:

$$\mathrm{L}_\lambda = \mathrm{M_L}{*}\mathrm{Q_{CAL}} + \mathrm{A_L}$$ (Eq. 5)

The band-specific multiplicative band number is represented by $\mathrm{M_L}$, $\mathrm{Q_{CAL}}$ is quantized and calibrated standard product pixel values, and $A_L$is the band-specific additive rescaling factor from the meta data. Using the thermal constants supplied in the metadata file, the TIRS band data should be converted from spectral radiance to brightness temperature (BT) after the digital numbers (DNs) are converted to reflection. The following Eq. 6 can be used to convert spectral radiation to brightness temperature (https://www.usgs.gov/landsat-missions/landsat-8).

$$\mathrm{BT} = \frac{\mathrm{k_2}}{\ln\left(\frac{\mathrm{k_1}}{\mathrm{L_\lambda}} + 1\right)} - (273.15)$$ (Eq. 6)

where $K1$ and $K2$ stand for the band-specific thermal conversion constants from the meta.

The radiant temperature is accomplished by adding absolute zero to get the results in Celsius (approx. −273.15◦ C) (H. Q. Xu & Chen, 2004)

2.4.1 NDVI Method for Emissivity Correction

Equation 7 describes how to calculate NDVI using the Near-Infrared (NIR) and Red (R) bands. NDVI, which has a range of -1 to + 1, measures the amount of vegetation present. Positive values represent areas with vegetation, whereas negative values denote areas without vegetation and bodies of water (Silleos et al., 2006).

$$\mathrm{NDVI} = \frac{\rho_{\mathrm{NIR}} - \rho_{\mathrm{red}}}{\rho_{\mathrm{NIR}} + \rho_{\mathrm{red}}}$$ (Eq. 7)

The reflectance band in the NIR region is denoted by the symbol ρ_{NIR}, while the reflectance band in the Red region is denoted by the symbol ρ_{red}. P_v denotes the percentage of vegetation which is determined by applying the Eq. 8 (Sultana & Satyanarayana, 2020).

$$\mathrm{P_v} = \left[\frac{\mathrm{NDVI} - \mathrm{NDVI_{min}}}{\mathrm{NDVI_{max}} - \mathrm{NDVI_{min}}}\right]^2$$ (Eq. 8)

$NDVI_{max}$ is the maximum DN values from NSVI image, and $NDVI_{min}$ is the minimum DN values from NDVI image.

The calculation of surface emissivity was the next stage (E) to estimate LST (Dwivedi & Khire, 2018; Meng et al., 2019), and the percentage of vegetation (PV) was used to compute it. The parameter (E) was calculated using the next Eq. 9 (Mujabar, 2019)

Land surface emissivity $(E) = 0.004 * PV + 0.986$ (Eq. 9)

2.4.2 Estimation of LST

The final stage was calculating LST using the following Eq. 10 shown below (Reddy et al., 2017; Sultana & Satyanarayana, 2020)

$$\mathrm{LST} = \frac{\mathrm{BT}}{\left[1 + \left\{\left(\mathrm{L_\lambda} * \frac{\mathrm{BT}}{\rho}\right) * \ln\epsilon\right\}\right]}$$ (Eq. 10)

Where,

LST = Land surface temperature;

ρ = h∗c/ σ =emitted radiance: (ρ = h ∗ c/σ = 1.438 ∗ 10 − 2 Mk);

ε = the land surface emissivity (LSE)

2.5 Extraction of spectral indices

Land cover indices, also known as spectral indices, are crucial sources for the precise measurement of LST. Spectral indices including NDVI, SAVI, MNDWI, and NDBI have been derived for the years 2012, 2017, and 2022 (Fig. 6). The names, formulas and the references of these spectral indices are presented in Table 2.

Table 2
Equation or LULC indices

Index Name and Abbreviation	Formula for Landsat	Reference
NDVI	$\frac{NIR-Red}{NIR+Red}$	(Rouse Jr et al., 1973)
NDBI	$\frac{SWIR-NIR}{SWIR+NIR}$	(Zha et al., 2003)
SAVI	$\frac{NIR-Red}{NIR+Red+0.5}(1+0.5)$	(Huete, 1988)
MNDWI	$\frac{Green-MIR}{Green+MIR}$	(H. Xu, 2006)

For evaluating vegetative health, NDVI and SAVI are crucial metrics. (Wilson et al., 2016). To adjust for the soil brightness impact where there is little plant cover, the SAVI was proposed as a modification of the NDVI (Huete, 1988). MNDWI is essential for managing surface water resources and monitoring drought (Sekertekin et al., 2018). For built-up area extraction, NDBI is one of the most popular indices (Sekertekin & Marangoz, 2017)

2.6 Statistical analysis

The goal was to conduct correlation analyses between LST and the spectral indices to find a statistically significant best-fit regression model for each year. The Akaike information criterion (AIC) and the Variance Inflation Factor (VIF) provided and verified the desired model. Finally, an extensive analysis of ordinary least square (OLS) multiple linear regression (MLR) (Hishe et al., 2017; Kumari et al., 2018; Yang et al., 2020), (Heinl et al., 2015) along with the relative importance (RI) of the individual independent parameters presented the results. All the statistical analyses and graphs have been done using R 4.2.0.

3 Results

3.1 Analysis of LULC mapping

The supervised classification approach was used for the LULC classification, and the results of classifying LULC are collated and displayed below. (Fig. 3, Table 3)

Table 3
Area coverage of each land cover class in the city of Balurghat (2012–2022).

LU/LC Classes	2012	2017	2022
	Percentage (%)	Percentage (%)	Percentage (%)
Waterbodies	3	5	5
Vegetation	64	60	44
Built-up	14	22	39
Sand	2	1	1
Bare land	5	2	1
Agricultural fallow land	12	10	10
TOTAL	100	100	100

Six categories of LULC, including waterbodies, vegetation, built-up regions, sand regions, bare land, and agricultural fallow land, were derived from the output maps of the classified images for the research period (2012–2022) (Table A1). To evaluate the quality of classification, an accuracy assessment has been performed. Overall Accuracies for classified images were 88.37%, 91.03%, and 96.02% for 2012, 2017, and 2022, respectively. In addition to this, Kappa coefficient values were 81.75%, 86.22%, and 94.61% for 2012, 2017, and 2022, respectively. Hence, the possibility of doing further research can be done by the result of accuracy assessment.

3.2 Analysis of change detection

Throughout the period from 2012 to 2022, a notable change in LULC from one class to another has been seen. Between 2012 and 2017, the built-up area and waterbodies increased by 8% and 2%, respectively. On the other hand, vegetation, bare land, sandy regions, and agricultural fallow land decreased by 4%, 3%, 1%, and 2%, respectively. Between 2017 and 2022, the only built-up area increased by 17%, bare land decreased by 1%, and vegetation decreased by 16%.

Agricultural fallow land, sand regions, and waterbodies remained unaltered. Overall the built-up area has increased while the vegetation-covered land has decreased as a result of urbanization from 2012 to 2022.

3.3 Impact of LULC change on LST

For each research period, the spatial analyst tool in ArcGIS 10.8 was used to do a spatial statistical analysis to provide LST values for various LULC classes. The obtained results showed that there are considerable differences in the mean LST values across different LULC classes and different geographical locations (Fig. 5). LST ranged from 19.09°C to 26.19°C in 2012, from 21.02°C to 26.46°C in 2017, and from 17.71 °C to 22.11°C in 2022. The mean LST in the study area was 22.76°C, 23.42°C, and 20°C, respectively. After an increase in LST from 2012 to 2017, the temperature marginally decreased in 2022. Reduced anthropogenic emissions and air pollutants owing to the stringent containment methods for controlling the COVID-19 virus on a global scale have various positive environmental consequences (Maithani et al., 2020; Ranjan et al., 2021). Due to the lockdown, there is a temporary shift in LST that offers a solid empirical foundation for future environmental benefits through urban design and policy implementation (Bera et al., 2021). In this study, the highest temperature was found in built-up areas and bare ground, while the lowest temperature was found where the waterbodies were located (Table 4).

Table 4
Mean values of LST (°C) under different LULC classes (2012–2022)

LU/LC Classes	2012 mean temperature (°C)	2017 mean temperature (°C)	2022 mean temperature (°C)
Waterbodies	19.58	21.56	17.85
Vegetation	22.52	23.37	19.72
Built-up	23.64	24.11	20.6
Sand	24.24	23.46	20.6
Bare land	24.54	24.96	20.79
Agricultural fallow land	22.68	22.69	19.85

According to the findings of the LULC change, it can be deduced that the built area rose steadily over 10 years, and this land use increased LST over the study periods. The LULC classes have a significant spatiotemporal impact on the LST pattern of the study area (Q. Sun et al., 2010).

3.4 Correlation analysis

NDVI has a slight positive correlation with LST, with R^2 values of 0.03 in 2017, while in 2012 and 2022, R^2 was 0.10 and 0.14, respectively (Fig. 4). LST and SAVI scatterplots have a striking pattern resemblance to LST and NDVI scatterplots. NDBI has a stronger relationship with LST than NDVI and SAVI. R^2 declined steadily during the research period, reaching 0.36 in 2022. In contrast to the other chosen variables, the scatterplots depicting the relationship between LST and MNDWI demonstrate a moderately negative connection.

3.4.1 Correlation among independent variables

The correlation table depicts a correlation of 1 between SAVI and NDVI over the years (Table.A2). Therefore, only NDVI is used for the subsequent calculations, as NDVI gives a better AICc score than SAVI when combined with other parameters. In 2012, the correlation between NDBI and MNDWI was 0.86. The finding may have hurt the significance of the regression analysis. Hence, we have ignored their connection in the subsequent calculation.

3.4.2 Selection of regression model

Table 5
Comparisons among models in terms of Adjusted R^2, RSE, VIF, AICc scores, F-statistics, and p-value

Year						2012
VARIABLES	ADJUSTED R^2	RSE	VIF	AICc	F	p
NDVI, SAVI, NDBI, MNDWI	0.63	0.67	NDVI: 1713 SAVI: 1717 NDBI: 64.41 MNDWI: 100.7	228.18	45.73	< 0.05
NDVI, MNDWI	0.61	0.68	1.61	229.93	85.11	< 0.05
MNDWI	0.58	0.71	-	237.82	147.2	< 0.05
NDVI, NDBI	0.57	0.72	1.09	240.17	72.67	< 0.05
NDBI	0.57	0.72	-	240.71	140.5	< 0.05
NDVI	0.09	1.05	-	320.34	11.91	< 0.05

Year						2017
VARIABLES	ADJUSTED R^2	RSE	VIF	AICc	F	p
NDVI, NDBI, MNDWI	0.55	0.61	NDVI: 42.40 NDBI: 57.62 MNDWI: 80.86	207.46	45.36	< 0.05
NDVI, SAVI, NDBI, MNDWI	0.55	0.62	NDVI: 2447 SAVI: 2447 NDBI: 57.63 MNDWI: 81.00	209.43	33.84	< 0.05
NDVI, MNDWI	0.54	0.62	1.45	210.01	63.48	< 0.05
NDBI, MNDWI	0.52	0.63	1.98	213.44	59.86	< 0.05
NDVI, NDBI	0.50	0.65	1.04	218.19	55.02	< 0.05
MNDWI	0.48	0.66	-	222.47	98.52	< 0.05
NDBI	0.41	0.70	-	234.53	76.92	< 0.05
NDVI	0.02	0.91	-	290.08	3.37	0.07

Year						2022
VARIABLES	ADJUSTED R^2	RSE	VIF	AICc	F	p
NDVI, NDBI, MNDWI	0.51	0.52	NDVI: 37.77 NDBI: 33.19 MNDWI: 73.01	173.43	38.4	< 0.05
NDVI, MNDWI	0.50	0.53	2.20	173.89	55.46	< 0.05
NDVI, SAVI, NDBI, MNDWI	0.51	0.53	NDVI: 3262 SAVI: 3262 NDBI: 33.94 MNDWI: 74.07	175.22	28.75	< 0.05
NDBI, MNDWI	0.49	0.53	1.94	176.50	52.88	< 0.05
MNDWI	0.47	0.55	-	180.35	95.26	< 0.05
NDVI, NDBI	0.47	0.55	1.00	181.13	48.46	< 0.05
NDBI	0.35	0.60	-	201.44	59.56	< 0.05
NDVI	0.13	0.7	-	233.41	17.14	< 0.05

The linear regression model of LST with NDVI and MNDWI provides the best and most credible explanation for all data sets throughout the specified timeframe (Table 5). We consistently obtained the same outcome by selecting models with the lowest AICc scores and eliminating them based on their VIFs > 2.5.

In 2012, multiple regression between NDVI, SAVI, NDBI, and MNDWI had the lowest AICc scores. Additionally, it has the highest adjusted R^2 of 0.63 and the lowest residual standard error. The model is statistically significant if its F-statistic is strong and its p-value is less than 0.05. However, the model has a high degree of multicollinearity with a VIF > 2.5, rendering the findings unreliable. Multiple Regression between NDVI and MNDWI with LST ranked second based on AICc, adjusted R^2, and RSE; it has a high F-statistic of 85.11, a p-value of less than 0.05, and a VIF of less than 2.5. MNDWI and NDVI combine to provide the best model to predict similar datasets for all the years. When comparing this model to others having minimal errors and high adjusted R^2 values, it consistently has the optimum adjusted R^2 with negligible error.

$$2012: \mathrm{LST} = 19.25 - 4.2\mathrm{NDVI} - 6.8\,\mathrm{MNDWI}$$

$$2017: \mathrm{LST} = 23.30 - 5.22\mathrm{NDVI} - 10.51\,\mathrm{MNDWI}$$

$$2022: \mathrm{LST} = 19.99 - 3.49\,\mathrm{NDVI} - 7.62\,\mathrm{MNDWI}$$

where:

LST is the land surface temperature (degrees Celsius);

NDVI is normalized difference vegetation index

MNDWI is the modified normalized difference water index

The NDVI coefficient climbed from 4.2 to 5.22 between 2012 and 2017 while plummeting to 3.49 in 2022. This fall demonstrated a change in the direction consistent with the prior results. The findings suggest that water and vegetation in the research region work to reduce the warming effect, where NDVI generally demonstrates a weaker impact on LST than MNDWI.

3.4.3 Assumptions of linear regression

Until this point, the approach has focused on the methods and results of linear regression. The next step in the process is to determine whether the models follow the fundamental statistical assumptions for linear regression (Fig. 7). The residual vs. fitted scatterplots exhibit neither a parabolic pattern nor a funnel shape, concluding that the models are homoscedastic and linear. Furthermore, we conducted a studentized Breusch-Pagan test for each year where p = 0.80, 0.16, and 0.40 in 2012, 2017, and 2022, respectively, confirming homoscedasticity. The q-q or quantile-quantile scatter plots do not display a curve line; this leads us to conclude that the data is normally scattered. The scale location plot suggest that errors are regularly distributed as there is no obvious pattern in these plots (usually like a funnel shape). Cases have an impact on the findings of the regression when they are outside of Cook's distance. We can use the entire dataset for subsequent calculations as none of the outliers from 2012 to 2022 are outside the dashed line or Cook's distance.

The successive correlations in all the graphs from 2012 to 2022 decline swiftly to zero and remain (usually) within the boundaries of the significance level (dashed blue lines) after the lag-0 correlation (Fig. 8). As a result, the model is more effective and significant because the residuals of this model do not exhibit autocorrelation.

3.4.4 Ordinary linear regression analysis and relative importance analysis

Table 6
Results of the OLS MLR and RI analysis. Dependent Variable: LST.

2012	**OLS MLR analysis**				**RI analysis**	
Variables	Unstandardized Coefficients		Standardized β	Sig.	Raw Importance	Rescaled Importance (%)
	β	Standard Error				
CONSTANT	19.25	0.22		0.00		
NDVI	-4.20	1.31	-0.24	0.00	0.069	11.2
MNDWI	-6.82	0.57	-0.91	0.00	0.549	88.8
R^2 = 0.62; Adjusted R^2 = 0.61				*Total*:	0.618	100.0

2017	**OLS MLR analysis**				**RI analysis**	
Variables	Unstandardized Coefficients		Standardized β	Sig.	Raw Importance	Rescaled Importance (%)
	β	Standard Error				
CONSTANT	23.30	0.17		0.00		
NDVI	-5.22	1.34	-0.31	0.00	0.048	8.8
MNDWI	-10.51	0.96	-0.87	0.00	0.499	91.2
R^2 = 0.55; Adjusted R^2 = 0.54				*Total*:	0.547	100.0

2022	**OLS MLR analysis**				**RI analysis**	
Variables	Unstandardized Coefficients		Standardized β	Sig.	Raw Importance	Rescaled Importance (%)
	β	Standard Error				
CONSTANT	19.99	0.14		0.00		
NDVI	-3.49	1.18	-0.30	0.00	0.090	17.5
MNDWI	-7.62	0.85	-0.91	0.00	0.424	82.5
R^2 = 0.51; Adjusted R^2 = 0.50				*Total*:	0.514	100.0

The model containing NDVI and MNDWI explained 61.8% of the data containing LST in 2012 (Table 6). The following ten years saw a slow reduction until it reached about 51.4% in 2022. The RI of the effects of MNDWI rose from 88.8–91.2% from 2012 to 2017 while it decreased to 82.5% in 2022. In contrast,

NDVI fell from 11.2–8.8% in 2017 and increased to 17.5% in 2022. The increased NDVI in 2022 can be related to the post-COVID period with reduced pollution levels.

4 Discussion

4.1 Trends in LULC

Results indicate a significant increase in urbanization between 2012 and 2022, with a decrease in vegetation (64–44%) and an increase in built-up areas (14–39%). However, not all of the vegetation-covered region has been turned into a built-up area. Modifications in LULC brought on by the rapid population expansion and corresponding rise in anthropogenic activities are the primary forces behind the environmental changes (Rahman et al., 2011). (Munthali et al., 2019). The LULC shift during the research period caused the mean LST to rise from 2012 to 2017 before it declined in 2022. Even though in 2022, vegetation is at an all-time low and urbanization is at an all-time high, it is worth noting that water body percentage is the highest and barren land percentage is the lowest. This condition is crucial since we learned that barren terrain has the highest LST mean while waterbodies have the least. This situation, combined with the decline in pollution following the lockdown period, intensified their impact on LST in 2022. (Demongeot et al., 2020) demonstrates that the temperature had fallen as a result of the lockdown. Earlier, the continuous emission of pollutants may have obscured these consequences.

4.2 Correlation between LST and individual spectral indices

The correlations between NDVI and LST are generally positive in winter and spring, negative in summer, and insignificant in autumn (Guha et al., 2022; Marzban et al., 2018). (D. Sun & Kafatos, 2007). The 2017 data was taken in late February, closer to spring. On the other hand, the 2012 and 2022 data were obtained earlier in the month, resulting in a higher positive association due to proximity to winter. Over the years, NDVI and SAVI have maintained a consistent correlation with LST while the temporal fluctuations in MNDWI are inversely comparable to those between LST and NDBI.

4.3 Interactions among the independent parameters

Any time there's a low vegetation cover, NDVI will be sensitive to the soil, which can confound measurements. On the other hand, where there's a large amount of vegetation, NDVI tends to saturate; SAVI in such situations provides superior results (Jiang et al., 2007; Qi et al., 1994). As there has been a significant decrease in the vegetation cover, it would be natural to expect changes in NDVI and SAVI. However, the correlation between them remained 1, from 2012 to 2022—this implies the reduction in vegetation cover has not led to interference in the uniform distribution of healthy vegetation throughout. The R^2 between NDBI and MNDWI was very high in 2012, with the lowest area of open water sources and built-up. Over the years, the rate of expansion of these features has varied. This situation led to the fall in the correlation between the two indices in 2017 and 2022 (Table A2).

4.4 Model selection and verification

Except for 2022, all the years with high R^2 also have low AICc scores. In 2022, the model with the third-lowest AICc score outperforms the model with the second-lowest AICc value in terms of R^2. Here, the AIC model selection approach has been chosen over R^2 to find the best-fit model since a lower AIC indicates improved prediction in a model while R^2 only measures how well a model fits the observed data.

Although there may be minimal to moderate correlation (0.01–0.5) between the independent variables according to the correlation matrix, it can still influence the model's correctness. Hence, VIF was used to verify how much the remaining multicollinearity inflates the variance of the regression coefficient. Even with $p < 0.05$, multicollinearity might harm the regression findings (Dodge, 2008).

4.5 Regression analysis

For ten years, all the chosen models from each year explain around half of the variations in LST, in which MNDWI consistently contributes more than 80 percent-this condition is in line with the fact that the town of Balurghat was historically constructed around the Atrai river, making it the most significant body of open water and primary feature. The literature (Le Phuc et al., 2022; Murakawa et al., 1991) acknowledges that rivers passing by urban areas may regulate the urban climate. The Atrai river is valuable to the people of Balurghat since it is the only river to originate from the region, serves as a source of irrigation, a year-round fishing spot and is a conduit for export commerce when it rains. The findings indicate that the river's influence on the town's local climatic variations and changes is still rather significant. This setting agrees with the situation in Nanjing, Wuhan, and Chongqing, where the Yangtze River substantially influences the temperature of the land surface (Wang et al., 2020).

Due to the complexities among the independent parameters within the limited space, the conclusions of this paper specifically reflect the relationships between LST and several spectral indices in a small developing riverine town. Therefore, the holistic implications of the underlying hydrologic, meteorologic, and anthropologic activities will be the focus of future work.

5 Conclusion

Due to global warming, the LST has recently experienced a surge. This localized study examines the LST changes in Balurghat during the past ten years, from 2012 to 2022, in terms of LULC. In general, local temperature variations that might potentially result in climate change include the moderated effects of a significant body of water, such as rivers, over metropolitan areas. This study has shown some evidence that, despite the recent urbanization of the region, the Atrai river's existence has had a significant impact on the local climate of Balurghat town. The rise and drop in LST mean values over time have been affected by the LULC changes discussed in this work. The warming and rising mean from 2012 to 2017 and the subsequent cooling effect on the environment brought on by the lockdown post-pandemic in 2022, even though the terrain remained the same, provide stunning illustrations of the local climate change in this study. The study is an example of how, despite increasing urbanization, nature still holds the final word, dispelling several beliefs that the world is becoming

increasingly dependent on manufactured features. These natural features (waterbodies and vegetation in this case) should be protected and preserved. Urban development ought to sustain these natural riches in modest communities like Balurghat, which depend on the Atrai river for fundamental necessities. This paper provides a frame of reference for the change in climate conditions before and after the pandemic. For a deeper understanding of the underlying natural processes, more and more extensive and realistic analyses and models are encouraged. To develop the town more effectively, studies like this will forecast its future and focus on factors that have a spatiotemporal impact.

Declarations

Author Contributions

Conceptualization, C.S., S.S., A.G.; methodology, , C.S., S.S., A.G. ; software, , C.S., S.S., A.G; validation, , C.S., S.S., A.G; formal analysis, , C.S., S.S., A.G; investigation, , C.S., S.S., A.G; resources, , C.S., S.S., A.G.; data creation, , C.S., S.S.; writing—original draft preparation, , C.S., S.S. A.G. T.T.N, I.E., N.N.M; writing—review and editing, , C.S., S.S., A.G., T.T.N., I.E., N.N.M visualization, S.S.; supervision and revision, A.G., S.S; project administration, A.G., N.N.M; funding – T.T.N; All authors have read and agreed to the published version of the manuscript.

Funding: The authors are thankful to the Deanship of Scientific Research at Najran University for funding this work, under the Research Groups Funding program grant code (NU/RG/SERC/12/21).

Ethical Approval: Not applicable

Consent to Participate: Not applicable

Consent to Publish: Not applicable

Acknowledgment: The authors are thankful to the Deanship of Scientific Research at Najran University for funding this work, under the Research Groups Funding program grant code (NU/RG/SERC/12/21).

Competing Interests: This manuscript has not been published or presented elsewhere in part or entirety and is not under consideration by another journal. There are no conflicts of interest to declare.

Availability of data and materials: The data that support the findings of this study are available from the corresponding author, upon reasonable request.

References

1. AL-Shammari, M. M. A., AL-Shamma'a, A. M., Al Maliki, A., Hussain, H. M., Yaseen, Z. M., & Armanuos, A. M. (2021). Integrated Water Harvesting and Aquifer Recharge Evaluation Methodology Based on Remote Sensing and Geographical Information System: Case Study in Iraq. *Natural Resources Research*, *30*(3), 2119–2143. https://doi.org/10.1007/s11053-021-09835-3
2. Alexander, C. (2020). Normalised difference spectral indices and urban land cover as indicators of land surface temperature (LST). *Int J Appl Earth Obs Geoinformation*, *86*, 102013. https://doi.org/10.1016/j.jag.2019.102013
3. Alipour, T., M.R.Sarajian, & Esmaeily, A. (2003). Land surface temperature estimation from thermal band of Landsat sensor, case study: Alashtar City. *International Archives of the Photogrammetry Remote Sensing and Spatial Information Sciences*, *38*(4), 1–6. https://www.researchgate.net/profile/Tayeb-Alipour-Fard/publication/215444122_Land_surface_temperature_estimation_from_thermal_band_of_landsat_sensor_case_study_Alashtar_City/links/07e71a6d3262665ea5699425/Land-surface-temperature-estimation-from-thermal-
4. Balew, A., & Korme, T. (2020). Monitoring land surface temperature in Bahir Dar city and its surrounding using Landsat images. *The Egyptian Journal of Remote Sensing and Space Sciences*, *23*(3), 371–386. https://doi.org/10.1016/j.ejrs.2020.02.001
5. Battista, G., & Vollaro, R. D. L. (2017). Correlation between air pollution and weather data in urban areas: Assessment of the city of Rome (Italy) as spatially and temporally independent regarding pollutants. *Atmospheric Environment*, *165*, 240–247. https://doi.org/10.1016/j.atmosenv.2017.06.050
6. Bera, B., Bhattacharjee, S., Shit, P. K., Sengupta, N., & Saha, S. (2021). Significant impacts of COVID-19 lockdown on urban air pollution in Kolkata (India) and amelioration of environmental health. *Environment, Development and Sustainability*, *23*(5), 6913–6940. https://doi.org/10.1007/s10668-020-00898-5
7. Bogoliubova, A., & Tymków, P. (2014). ACCURACY ASSESSMENT OF AUTOMATIC IMAGE PROCESSING FOR LAND COVER CLASSIFICATION OF ST . PETERSBURG PROTECTED AREA. *Acta Scientiarum Polonorum, Administratio Locorum*, *13*(1–2), 5–22.
8. Carlson, T. N., & Sanchez-Azofeifa, G. A. (1999). Satellite remote sensing of land use changes in and around San Jose, Costa Rica. *Remote Sensing of Environment*, *70*(3), 247–256. https://doi.org/10.1016/S0034-4257(99)00018-8Get
9. Chakraborty, A., & Sehgal, V. K. (2010). Assessment of Agricultural Drought Using MODIS Derived Normalized Difference Water Index. *Journal of Agricultural Physics*, *10*, 28–36. https://doi.org/http://www.agrophysics.in/admin/adminjournalpdf/20181214132450528131903/journal-593476142.pdf
10. Daou, I., Mariko, A., Rasmus, F., Menenti, M., Kourosh, K., Maïga, H. B., & Maïga, S. M. (2012). Estimation and Mapping of Land Surface Temperature From AATSR Images And GIS : A Case Study In Kolondieba-Tiendaga Basin In Sudano-Sahelian Climate , Mali. *International Journal Of Computational Engineering Research*, *2*(5), 1567–1576. https://citeseerx.ist.psu.edu/viewdoc/download?doi=10.1.1.448.6161&rep=rep1&type=pdf
11. Demongeot, J., Flet-Berliac, Y., & Seligmann, H. (2020). Temperature decreases spread parameters of the new Covid-19 case dynamics. *Biology*, *9*(5), 94. https://doi.org/10.3390/biology9050094

12. Dezso, Z., Bartholy, J., Pongracz, R., & Barcza, Z. (2005). *Analysis of land-use / land-cover change in the Carpathian region based on remote sensing techniques*. *30*(1–3), 109–115. https://doi.org/10.1016/j.pce.2004.08.017
13. Dissanayake, D. M. S. L. B., Morimoto, T., Ranagalage, M., & Murayama, Y. (2019). Land-use/land-cover changes and their impact on surface urban heat islands: Case study of Kandy City, Sri Lanka. *Climate*, *7*(8), 99. https://doi.org/10.3390/cli7080099
14. Dodge, Y. (2008). The Concise Encyclopedia of Statistics. In *Springer Science & Business Media* (Vol. 38, Issue 4). https://doi.org/10.1080/02664760903075614
15. Donnell, E. M. O., Barsi, J. A., Schott, J. R., Palluconi, F. D., Helder, D. L., Hook, S. J., Markham, B. L., & Chander, G. (2003). Landsat TM and ETM + thermal band calibration. *Canadian Journal of Remote Sensing*, *29*(2), 141–153. https://doi.org/10.5589/m02-087
16. Dwivedi, A., & Khire, M. V. (2018). Application of Split- Window Algorithm to study Urban Heat Island Effect in Mumbai through Land Surface Temperature approach. *Sustainable Cities and Society*, *41*, 865–877. https://doi.org/10.1016/j.scs.2018.02.030
17. Eena, K. V, Arammasivam, K. M. P., & Enkatesh, T. N. V. (2020). Urban Heat Island studies : Current status in India and a comparison with the International studies. *Journal of Earth System Science*, *129*(1), 1–15. https://doi.org/10.1007/s12040-020-1351-y
18. Guha, S., Govil, H., Dey, A., & Gill, N. (2018). Analytical study of land surface temperature with NDVI and NDBI using Landsat 8 OLI and TIRS data in Florence and Naples city , Italy. *European Journal of Remote Sensing*, *51*(1), 667–678. https://doi.org/10.1080/22797254.2018.1474494
19. Guha, S., Govil, H., Taloor, A. K., Gill, N., & Dey, A. (2022). Land surface temperature and spectral indices: A seasonal study of Raipur City. *Geodesy and Geodynamics*, *13*(1), 72–82. https://doi.org/10.1016/j.geog.2021.05.002
20. Hao, X., Li, W., & Deng, H. (2016). The oasis effect and summer temperature rise in arid regions - case study in Tarim Basin. *Nature Publishing Group*, *6*(October), 1–9. https://doi.org/10.1038/srep35418
21. Heinl, M., Hammerle, A., Tappeiner, U., & Leitinger, G. (2015). Determinants of urban-rural land surface temperature differences - A landscape scale perspective. *Landscape and Urban Planning*, *134*, 33–42. https://doi.org/10.1016/j.landurbplan.2014.10.003
22. Hishe, S., Lyimo, J., & Bewket, W. (2017). Effects of soil and water conservation on vegetation cover: a remote sensing based study in the Middle Suluh River Basin, northern Ethiopia. *Environmental Systems Research*, *6*(1). https://doi.org/10.1186/s40068-017-0103-8
23. Huete, A. R. (1988). A Soil-Adjusted Vegetation Index (SAVI). *REMOTE SENSING OF ENVIRONMENT*, *25*(3), 295–309. https://doi.org/10.1016/0034-4257(88)90106-X
24. Ishola, K. A., Okogbue, E. C., & Adeyeri, O. E. (2016). Dynamics of surface urban biophysical compositions and its impact on land surface thermal field. *Modeling Earth Systems and Environment*, *2*(4), 1–20. https://doi.org/10.1007/s40808-016-0265-9
25. Jiang, Z., Huete, A. R., Li, J., & Qi, J. (2007). Interpretation of the modified soil-adjusted vegetation index isolines in red-NIR reflectance space. *Journal of Applied Remote Sensing*, *1*(1), 013503. https://doi.org/10.1117/1.2709702
26. Kalma, J. D., McVicar, T. R., & McCabe, M. F. (2008). Estimating Land Surface Evaporation : A Review of Methods Using Remotely Sensed Surface Temperature Data. *Surveys in Geophysics*, *29*(7), 421–469. https://doi.org/10.1007/s10712-008-9037-z
27. Kamilya, P., Das, A., Das, A., & Sarkar, A. (2015). Comparative analysis of major phenotypical traits of some Dicotyledonous weed seedlings of crop fields of Balurghat Block. *Dakshindinajpur, West Bengal*, *9*(1), 107–118. http://pleione.ehsst.org/journals/Pleione91/11 Weed Seedlings Dinajpur.pdf
28. Khandelwal, S., Goyal, R., Kaul, N., & Mathew, A. (2017). Assessment of land surface temperature variation due to change in elevation of area surrounding Jaipur, India. *The Egyptian Journal of Remote Sensing and Space Sciences*, *21*(1), 87–94. https://doi.org/10.1016/j.ejrs.2017.01.005
29. Kikon, N., Singh, P., Singh, S. K., & Vyas, A. (2016). Assessment of Urban Heat Islands (UHI) of Noida City, India using multi-temporal satellite data. *Sustainable Cities and Society*, *22*, 19–28. https://doi.org/10.1016/j.scs.2016.01.005
30. Kometa, S. S., & Akoh, N. R. (2012). The Hydro-geomorphological Implications of Urbanisation in Bamenda, Cameroon. *Journal of Sustainable Development*, *5*(6), 64–73. https://doi.org/10.5539/jsd.v5n6p64
31. Kumar, D., & Shekhar, S. (2015). Statistical analysis of land surface temperature–vegetation indexes relationship through thermal remote sensing. *Ecotoxicology and Environmental Safety*, *121*(2), 39–44. https://doi.org/10.1016/j.ecoenv.2015.07.004
32. Kumari, B., Tayyab, M., Shahfahad, Salman, Mallick, J., Khan, M. F., & Rahman, A. (2018). Satellite-Driven Land Surface Temperature (LST) Using Landsat 5, 7 (TM/ETM+ SLC) and Landsat 8 (OLI/TIRS) Data and Its Association with Built-Up and Green Cover Over Urban Delhi, India. *Remote Sensing in Earth Systems Sciences*, *1*(3–4), 63–78. https://doi.org/10.1007/s41976-018-0004-2
33. Kundu, P. K. (2018). EMERGENCE OF BALURGHAT AS A CLASS-I CITY : DEMOGRAPHIC IMPACT OF PARTITION AND BANGLADESH LIBERATION WAR. *INTERNATIONAL JOURNAL OF RESEARCH AND ANALYTICAL REVIEWS*, *5*(3), 955–964.
34. Le Phuc, C. L., Nguyen, H. S., Dao Dinh, C., Tran, N. B., Pham, Q. B., & Nguyen, X. C. (2022). Cooling island effect of urban lakes in hot waves under foehn and climate change. *Theoretical and Applied Climatology*, *149*(1–2), 817–830. https://doi.org/10.1007/s00704-022-04085-6
35. Li, W., Cao, Q., Lang, K., & Wu, J. (2017). Linking potential heat source and sink to urban heat island: Heterogeneous effects of landscape pattern on land surface temperature. *Science of the Total Environment*, *586*, 457–465. https://doi.org/10.1016/j.scitotenv.2017.01.191
36. Liu, H. Q., & Huete, A. (1995). A feedback based modification of the NDVI to minimize canopy background and atmospheric noise. *IEEE Transactions on Geoscience and Remote Sensing*, *33*(2), 457–465. https://doi.org/10.1109/TGRS.1995.8746027
37. Lundholm, J. T., & Richardson, P. J. (2010). Habitat analogues for reconciliation ecology in urban and industrial environments. *Journal of Applied Ecology*, *45*(5), 966–975. https://doi.org/10.1111/j.1365-2664.2010.01857.x
38. Maithani, S., Nautiyal, G., & Sharma, A. (2020). Investigating the Effect of Lockdown During COVID-19 on Land Surface Temperature : Study of Dehradun City , India. *Journal of the Indian Society of Remote Sensing*, *48*(9), 1297–1311. https://doi.org/10.1007/s12524-020-01157-w

39. Marzban, F., Sodoudi, S., & Preusker, R. (2018). The influence of land-cover type on the relationship between NDVI–LST and LST-Tair. *International Journal of Remote Sensing*, *39*(5), 1377–1398. https://doi.org/10.1080/01431161.2017.1402386
40. Mathew, A., Khandelwal, S., & Kaul, N. (2018). Spatio-temporal variations of surface temperatures of Ahmedabad city and its relationship with vegetation and urbanization parameters as indicators of surface temperatures. *Remote Sensing Applications: Society and Environment*, *11*, 119–139. https://doi.org/10.1016/j.rsase.2018.05.003
41. Meng, X., Cheng, J., Zhao, S., Liu, S., & Yao, Y. (2019). Estimating Land Surface Temperature from Landsat-8 Data using the NOAA JPSS Enterprise Algorithm. *Remote Sensing*, *11*(2), 155. https://doi.org/10.3390/rs11020155
42. Mujabar, P. S. (2019). Spatial-temporal variation of land surface temperature of Jubail Industrial City , Saudi Arabia due to seasonal effect by using Thermal Infrared Remote Sensor (TIRS) satellite data. *Journal of African Earth Sciences*, *155*, 54–63. https://doi.org/10.1016/j.jafrearsci.2019.03.008
43. Munthali, M. G., Davis, N., Adeola, A. M., Botai, J. O., Kamwi, J. M., Chisale, H. L. W., & Orimoogunje, O. O. I. (2019). Local perception of drivers of Land-Use and Land- Cover change dynamics across Dedza district, Central Malawi region. *Sustainability (Switzerland)*, *11*(3), 832. https://doi.org/10.3390/su11030832
44. Murakawa, S., Sekine, T., & Narita, K. ichi. (1991). Study of the effects of a river on the thermal environment in an urban area. *Energy and Buildings*, *16*(3–4), 993–1001. https://doi.org/10.1016/0378-7788(91)90094-j
45. Myint, S. W., Wentz, E. A., Brazel, A. J., & Quattrochi, D. A. (2013). The impact of distinct anthropogenic and vegetation features on urban warming. *Landscape Ecology*, *28*(5), 959–978. https://doi.org/10.1007/s10980-013-9868-y
46. Narasimhan, B., & Srinivasan, R. (2005). Development and evaluation of Soil Moisture Deficit Index (SMDI) and Evapotranspiration Deficit Index (ETDI) for agricultural drought monitoring. *Agricultural and Forest Meteorology*, *133*(1–4), 69–88. https://doi.org/10.1016/j.agrformet.2005.07.012
47. Nega, W., & Balew, A. (2022). The relationship between land use land cover and land surface temperature using remote sensing: systematic reviews of studies globally over the past 5 years. *Environmental Science and Pollution Research*, *29*(28), 42493–42508. https://doi.org/10.1007/s11356-022-19997-z
48. Neog, R., Acharjee, S., & Hazarika, J. (2019). Evaluation of spatio-temporal pattern of surface urban heat island phenomena at Jorhat, India. *Arabian Journal of Geosciences*, *12*(10), 1–10. https://doi.org/10.1007/s12517-019-4484-z
49. Nichol, J. E., & Hang, T. P. (2012). Temporal characteristics of thermal satellite images for urban heat stress and heat island mapping. *International Society for Photogrammetry and Remote Sensing*, *74*, 153–162. https://doi.org/10.1016/j.isprsjprs.2012.09.007
50. Qi, J., Chehbouni, A., Huete, A. R., Kerr, Y. H., & Sorooshian, S. (1994). A modified soil adjusted vegetation index. *Remote Sensing of Environment*, *48*(2), 119–126. https://doi.org/10.1016/0034-4257(94)90134-1
51. Quattrochi, D. A., & Luvall, J. C. (1999). Thermal infrared remote sensing for analysis of landscape ecological processes : methods and applications. *Landscape Ecology*, *14*(6), 577–598. https://doi.org/10.1023/A:1008168910634
52. Rahaman, S., Kumar, P., Chen, R., Meadows, M. E., & Singh, R. B. (2020). Remote Sensing Assessment of the Impact of Land Use and Land Cover Change on the Environment of Barddhaman District, West Bengal, India. *Frontiers in Environmental Science*, *8*, 1–15. https://doi.org/10.3389/fenvs.2020.00127
53. Rahman, A., Kumar, Y., Fazal, S., & Bhaskaran, S. (2011). Urbanization and Quality of Urban Environment Using Remote Sensing and GIS Techniques in East Delhi-India. *Journal of Geographic Information System*, *03*(01), 62–84. https://doi.org/10.4236/jgis.2011.31005
54. Rajendran, P., & Mani, K. (2015). Estimation of Spatial Variability of Land Surface Temperature using Landsat 8 Imagery. *The International Journal Of Engineering And Science*, *4*(11), 19–23. https://theijes.com/papers/v4-i11/Version-3/D041103019023.pdf
55. Ranjan, B., Bar, S., Kaskaoutis, D., Chandra, A., Polade, S. D., & Goswami, S. (2021). Impact of COVID-19 induced lockdown on land surface temperature , aerosol , and urban heat in Europe and North America. *Sustainable Cities and Society*, *75*(August), 103336. https://doi.org/10.1016/j.scs.2021.103336
56. Reddy, S. N., Manikiam, B., & Jeevalakshmi, D. (2017). Land Surface Temperature Retrieval from LANDSAT data using Emissivity Estimation. *International Journal of Applied Engineering Research*, *12*(20), 9679–9687. https://www.ripublication.com/ijaer17/ijaerv12n20_57.pdf
57. Rouse Jr, J. W., Haas, R. H., Schell, J. A., & Deering, D. W. (1973). Paper a 20. *In Third Earth Resources Technology Satellite-1 Symposium: The Proceedings of a Symposium Held by Goddard Space Flight Center at Washington, DC*, *351*, 309. https://books.google.co.in/books?hl=en&lr=&id=s4KOAAAAIAAJ&oi=fnd&pg=PA309&dq=MONITORING+VEGETATION+SYSTEMS+IN+THE+GREAT+PLAINS+WITH+ERTS&ots=G6b_0aT-jx&sig=bnLaa45uKNkgLvwrQ8QvVP8BZ3M&redir_esc=y#v=onepage&q=MONITORING VEGETATION SYSTEMS IN THE GREAT PLA
58. Sekertekin, A., Cicekli, S. Y., & Arslan, N. (2018). Index-Based Identification of Surface Water Resources Using Sentinel-2 Satellite Imagery. *2018 2nd International Symposium on Multidisciplinary Studies and Innovative Technologies (ISMSIT)*, 1–5. https://doi.org/10.1109/ISMSIT.2018.8567062
59. Sekertekin, A., & Marangoz, A. M. (2017). An Erdas Imagine Model To Extract Urban Indices Using Landsat 8 Satellite Imagery. *International Journal of Scientific & Technology Research*, *6*(1), 62–67. https://www.researchgate.net/profile/Aycan-Marangoz-2/publication/312595170_An_Erdas_Imagine_Model_To_Extract_Urban_Indices_Using_Landsat_8_Satellite_Imagery/links/5885b17c4585150dde4a717d Erdas-Imagine-Model-To-Extract-Urban-Indices-Using-Landsat-8-Sa
60. Shikwambana, L., Kganyago, M., & Mhangara, P. (2021). Temporal analysis of changes in anthropogenic emissions and urban heat islands during covid-19 restrictions in Gauteng province, South Africa. *Aerosol and Air Quality Research*, *21*(9). https://doi.org/10.4209/aaqr.200437
61. Silleos, N. G., Alexandridis, T. K., Gitas, I. Z., & Perakis, K. (2006). Vegetation indices: Advances made in biomass estimation and vegetation monitoring in the last 30 years. *Geocarto International*, *21*(4), 21–28. https://doi.org/10.1080/10106040608542399
62. Singh, B., & Sarkar, C. (2020). Monitoring Urban Growth and Detection of Land Use / Land Cover Change in Silchar City , Assam and Balurghat City , West Bengal. *International Journal of Innovative Technology and Exploring Engineering*, *3075*(8), 796–803. https://doi.org/10.35940/ijitee.H6656.069820

63. Singh, P., Kikon, N., & Verma, P. (2017). Impact of land use change and urbanization on urban heat island in Lucknow city, Central India. A remote sensing-based estimate. *Sustainable Cities and Society*, *32*, 100–114. https://doi.org/10.1016/j.scs.2017.02.018
64. Son, N. T., Chen, C. F., & Chen, C. R. (2020). Urban expansion and its impacts on local temperature in San Salvador, El Salvador. *Urban Climate*, *32*(March), 100617. https://doi.org/10.1016/j.uclim.2020.100617
65. Song, J., Du, S., Feng, X., & Guo, L. (2014). The relationships between landscape compositions and land surface temperature: Quantifying their resolution sensitivity with spatial regression models. *Landscape and Urban Planning*, *123*, 145–157. https://doi.org/10.1016/j.landurbplan.2013.11.014
66. Stroppiana, D., Antoninetti, M., & Brivio, P. A. (2014). Seasonality of MODIS LST over Southern Italy and correlation with land cover, topography and solar radiation. *European Journal of Remote Sensing*, *47*(1), 133–152. https://doi.org/10.5721/EuJRS20144709
67. Sultana, S., & Satyanarayana, A. N. V. (2020). Assessment of urbanisation and urban heat island intensities using landsat imageries during 2000 – 2018 over a sub-tropical Indian City. *Sustainable Cities and Society*, *52*(May 2019), 101846. https://doi.org/10.1016/j.scs.2019.101846
68. Sun, D., & Kafatos, M. (2007). Note on the NDVI-LST relationship and the use of temperature-related drought indices over North America. *Geophysical Research Letters*, *34*(24), 1–4. https://doi.org/10.1029/2007GL031485
69. Sun, Q., Tan, Æ. J., & Xu, Æ. Y. (2010). An ERDAS image processing method for retrieving LST and describing urban heat evolution : a case study in the Pearl River Delta Region in South China. *Environmental Earth Sciences*, *59*(5), 1047–1055. https://doi.org/10.1007/s12665-009-0096-3
70. Thakur, S., Maity, D., Mondal, I., Basumatary, G., Ghosh, P. B., Das, P., & De, T. K. (2021). Assessment of changes in land use, land cover, and land surface temperature in the mangrove forest of Sundarbans, northeast coast of India. *Environment, Development and Sustainability*, *23*(2), 1917–1943. https://doi.org/10.1007/s10668-020-00656-7
71. Turner, B. L., Lambin, E. F., & Reenberg, A. (2007). The emergence of land change science for global environmental change and sustainability. *Proceedings of the National Academy of Sciences*, *104*(52), 20666–20671. https://doi.org/10.1073/pnas.070411910
72. Uddin, M. A., Kamal, A. S. M. M., & Shahid, S. (2022). Vegetation response to climate and climatic extremes in northwest Bangladesh: a quantile regression approach. *Theoretical and Applied Climatology*, *148*(3–4), 985–1003. https://doi.org/10.1007/s00704-022-03968-y
73. Vani, M., & Prasad, P. R. C. (2020). Assessment of spatio-temporal changes in land use and land cover, urban sprawl, and land surface temperature in and around Vijayawada city, India. *Environment, Development and Sustainability*, *22*(4), 3079–3095. https://doi.org/10.1007/s10668-019-00335-2
74. Wang, L., Hou, H., & Weng, J. (2020). Ordinary least squares modelling of urban heat island intensity based on landscape composition and configuration: A comparative study among three megacities along the Yangtze River. *Sustainable Cities and Society*, *62*(2318), 102381. https://doi.org/10.1016/j.scs.2020.102381
75. Wilson, N. R., Norman, L. M., Villarreal, M., Gass, L., Tiller, R., Salywon, A., Wilson, N. R., Norman, L. M., Villarreal, M., Gass, L., & Tiller, R. (2016). Comparison of remote sensing indices for monitoring of desert cienegas. *Arid Land Research and Management*, *30*(4), 460–478. https://doi.org/10.1080/15324982.2016.1170076
76. Xu, H. (2006). Modification of normalised difference water index (NDWI) to enhance open water features in remotely sensed imagery. *International Journal of Remote Sensing*, *27*(14), 3025–3033. https://doi.org/10.1080/01431160600589179
77. Xu, H. Q., & Chen, B. Q. (2004). Remote sensing of the urban heat island and its changes in Xiamen City of SE China. *Journal of Environmental Sciences*, *16*(2), 276–281. https://www.researchgate.net/publication/8567631_Remote_sensing_of_the_urban_heat_island_and_its_changes_in_Xiamen_City_of_SE_China
78. Yang, G., Yu, Z., Jørgensen, G., & Vejre, H. (2020). How can urban blue-green space be planned for climate adaption in high-latitude cities? A seasonal perspective. *Sustainable Cities and Society*, *53*, 101932. https://doi.org/10.1016/j.scs.2019.101932
79. Yue, W., Xu, J., Tan, W., & Xu, L. (2007). International Journal of Remote The relationship between land surface temperature and NDVI with remote sensing : application to Shanghai Landsat 7 ETM + data. *International Journal of Remote Sensing*, *28*(15), 3205–3226. https://doi.org/10.1080/01431160500306906
80. Zha, Y., Gao, J., & S.Ni. (2003). Use of normalized difference built-up index in automatically mapping urban areas from TM imagery. *International Journal of Remote Sensing*, *24*(3), 583–594. https://doi.org/10.1080/01431160304987

Figures

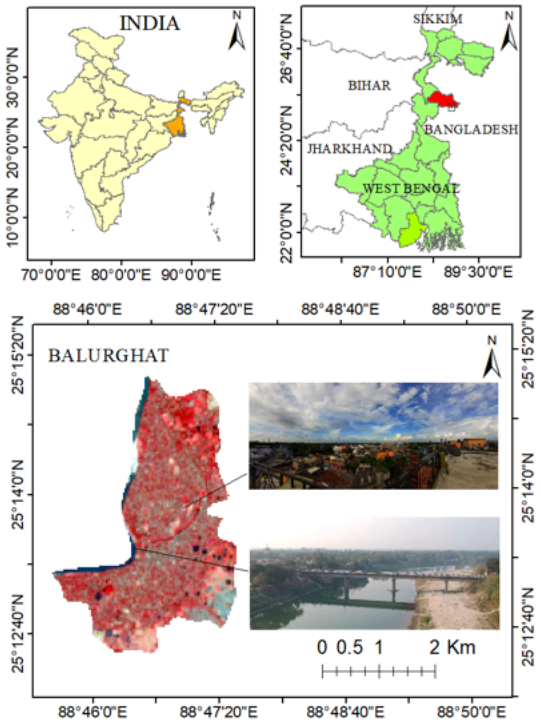

Figure 1

Location of the study area

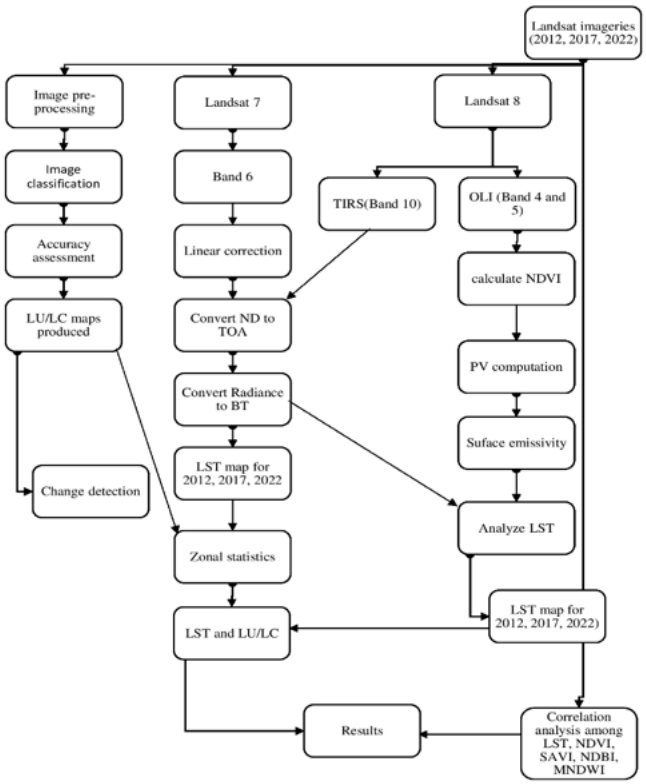

Figure 2

The Study's Methodology

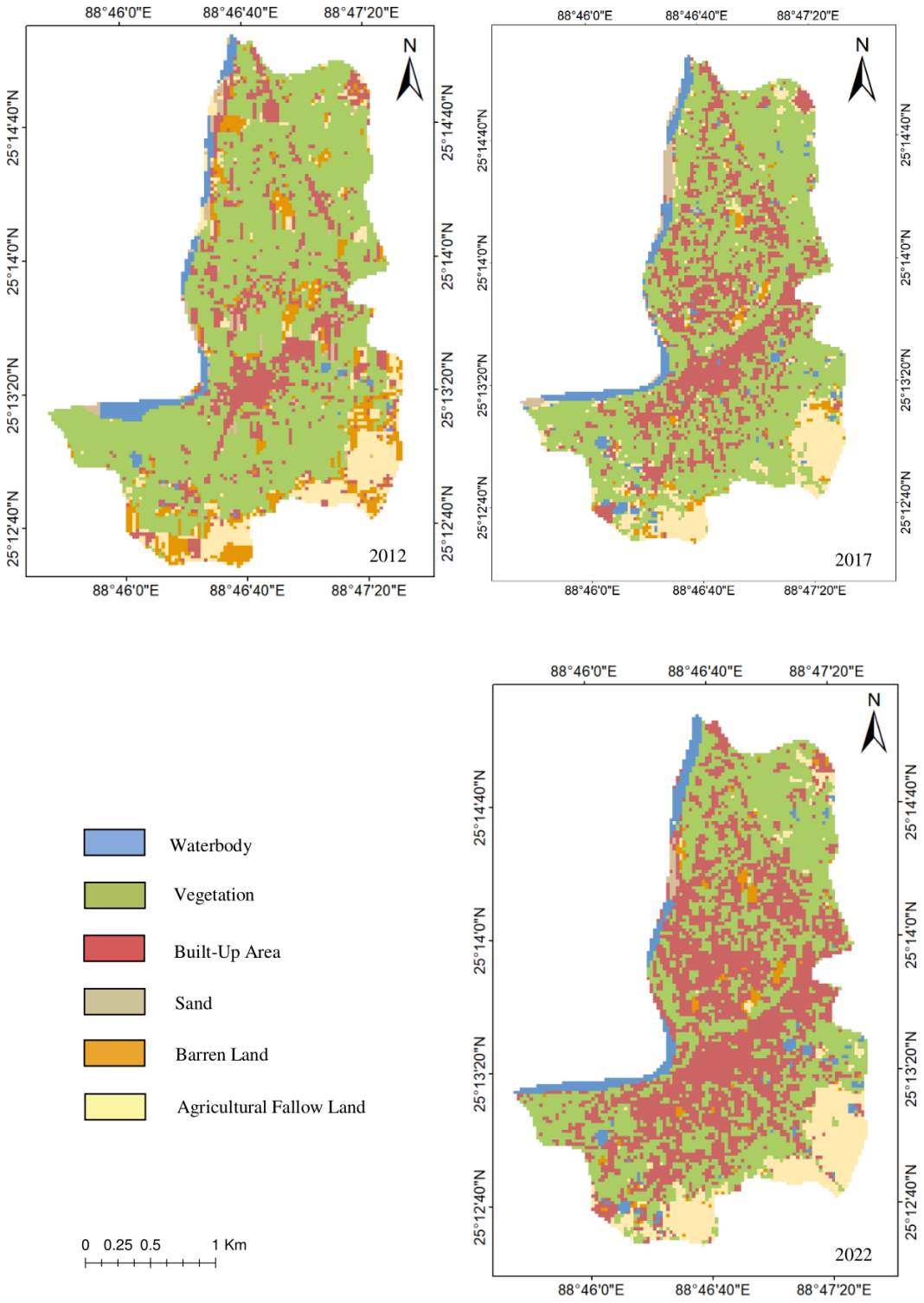

Figure 3

LULC classes of the study area in 2012, 2017, and 2022

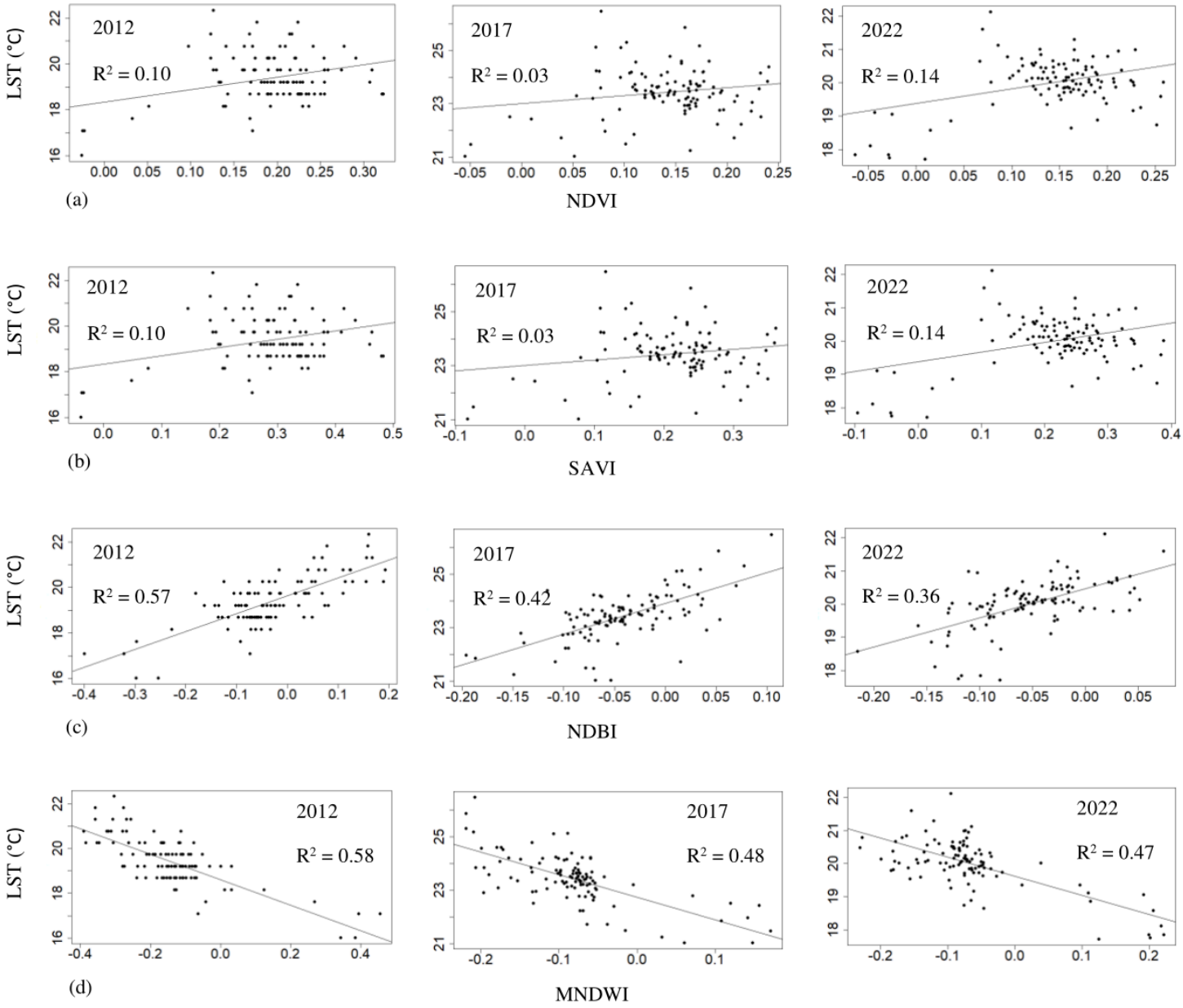

Figure 4

Scatterplots showing the correlation between LST and independent variables; (a) NDVI (b) SAVI (c) NDBI (d) MNDWI

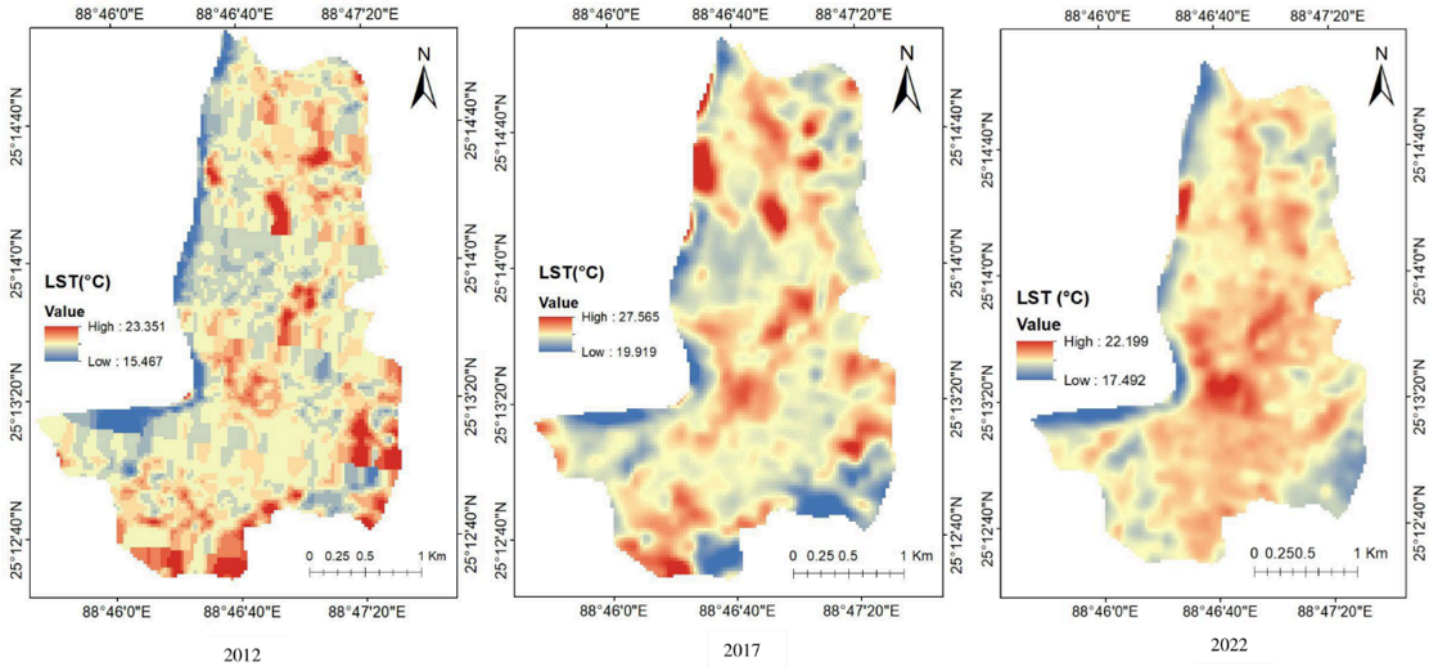

Figure 5

LST maps from 2007 to 2022

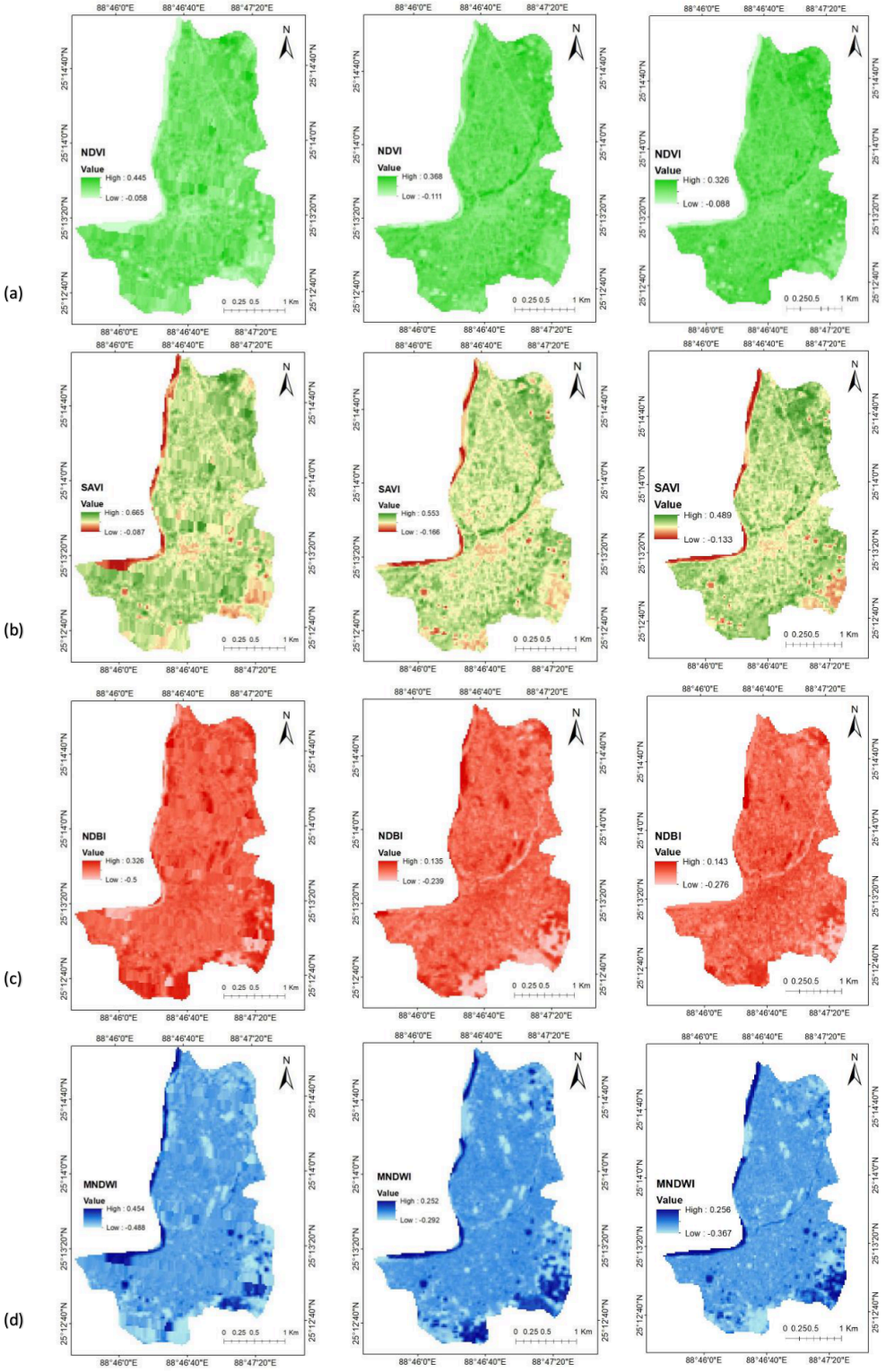

Figure 6

Different spectral indices map from 2007 to 2022 (left to right): (a) NDVI map; (b)

NDBI map (c) SAVI map; (d) MNDWI map

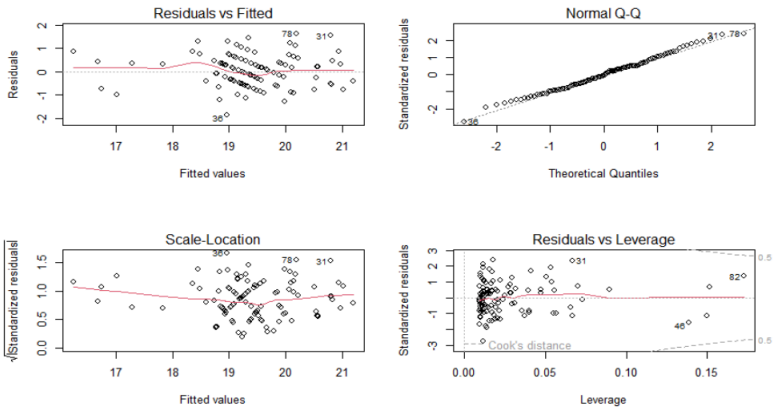

2012

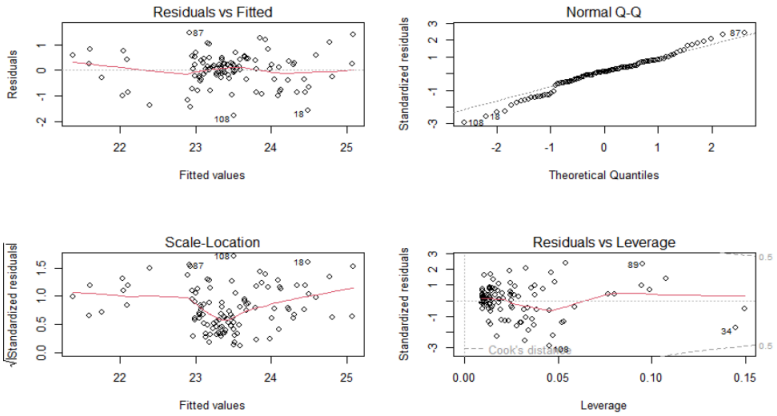

2017

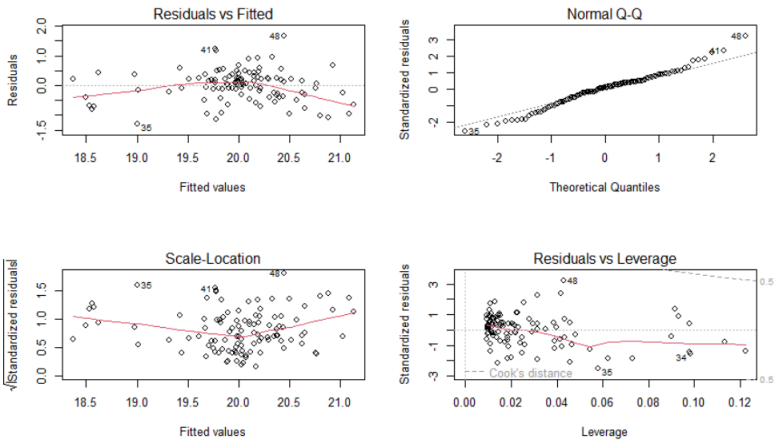

2022

Figure 7

Representation of residuals vs fitted, normal q-q, scale-location and residuals vs leverage plots (2012-2022)

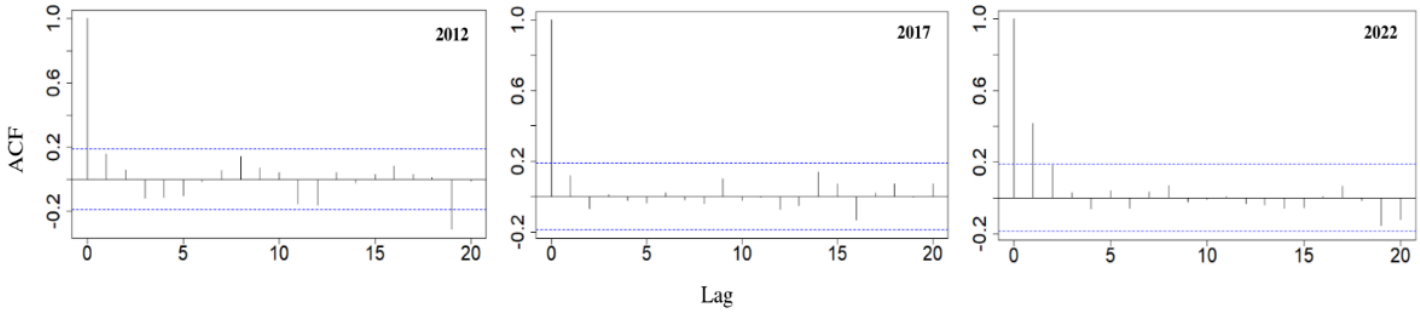

Figure 8

Representation of plots showing no autocorrelation (2012-2022)

Supplementary Files

This is a list of supplementary files associated with this preprint. Click to download.

- Appendix.docx